Evidence from galactic cosmic rays that the sun has likely entered a secular minimum in solar activity

Space Weather

RESEARCH ARTICLE
10.1029/2021SW002796

Evidence From Galactic Cosmic Rays That the Sun Has Likely Entered a Secular Minimum in Solar Activity

F. Rahmanifard[1,2], A. P. Jordan[1,2], W. C. de Wet[1,2], N. A. Schwadron[1,2], J. K. Wilson[1,2], M. J. Owens[3], H. E. Spence[1,2], and P. Riley[4]

[1]Space Science Center, University of New Hampshire, Durham, NH, USA, [2]Solar System Exploration Research Virtual Institute, NASA Ames Research Center, Moffett Field, CA, USA, [3]Department of Meteorology, Space and Atmospheric Electricity Group, University of Reading, Reading, UK, [4]Predictive Science, San Diego, CA, USA

Key Points:

- Trends observed in the modulation of galactic cosmic rays suggest that the Sun might be in a secular minimum
- The next two cycles will probably be weaker than average
- Cycle 25 will be as weak as or weaker than cycle 24

Correspondence to:

F. Rahmanifard,
F.Rahmanifard@unh.edu

Citation:

Rahmanifard, F., Jordan, A. P., de Wet, W. C., Schwadron, N. A., Wilson, J. K., Owens, M. J., et al. (2022). Evidence from galactic cosmic rays that the Sun has likely entered a secular minimum in solar activity. *Space Weather*, *20*, e2021SW002796. https://doi.org/10.1029/2021SW002796

Received 29 MAR 2021
Accepted 2 DEC 2021

Abstract Since the beginning of the space age, the Sun has been in a multi-cycle period of elevated activity (secular maximum). This secular maximum is the longest in the last 9300 years. Since the end of solar cycle 21 (SC21), however, the Sun has shown a decline in overall activity, which has remarkably increased the fluxes of galactic cosmic rays (GCRs). Here, we investigate the correlation between the modulation of GCRs, the heliospheric magnetic field, and solar wind speed for the last 24 solar cycles to find trends that can potentially be used to predict future solar activity. Specifically, we develop a tool for predicting future magnetic field intensity, based on the hysteresis in the GCR variation, during the last phases of the current cycle. This method estimates that SC25 will be as weak as or weaker than SC24. This would mean that the Sun has likely entered a secular minimum, which, according to historical records, should last for another two cycles (SC25 and SC26).

Plain Language Summary We investigated the correlation between the modulation of galactic cosmic rays (GCRs) and solar wind parameters to find trends that could be used in predicting future solar activity. Using this method, we estimate that SC25 will be as weak as or weaker than SC24. Furthermore, these trends suggest that the Sun might be in a secular minimum.

1. Introduction

Both sunspot numbers (SSN) and the heliospheric magnetic field (HMF) show approximately 11-year cycles that superpose longer-term quasi-periodic variations, called secular variations (for more information on solar cycles refer to Hathaway, 2010). Some of the more prominent secular variations are three grand minima: the Wolf (years 1280–1350), Maunder (years 1645–1710), and Dalton minima (years 1790–1830, solar cycles 6–8). In addition, the space age has coincided with the longest grand maximum in 9300 years (Abreu et al., 2008). But the duration of previous maxima and the quasi-periodic recurrence of these secular variations suggests that this grand maximum is ending, and the Sun is entering a possible grand minimum–a modern minimum.

While the 11-year solar cycles have been known for over a century, the physics behind it is not fully agreed-upon (Charbonneau, 2010). Variations of the solar magnetic field can be qualitatively described based on the oscillatory exchange of energy between poloidal and toroidal solar magnetic field components as a driving force for solar cycles. In this model, the toroidal magnetic field is generated by buoyant upwelling within the convective zone, which is itself created by the differential rotation of the Sun stretching the large-scale poloidal component and appears as bipolar magnetic regions (BMRs) on the Sun's surface. The effect of Coriolis force on the rising toroidal magnetic flux tubes tilts these BMRs, and turbulent convection further leads to a dispersion around the mean tilt. The poloidal component of the solar magnetic field and the resulting active regions reach their maximum during solar maximum. A poloidal dipolar field, on the other hand, is created by the shift of energy from the toroidal field to the poloidal field due to the dispersion and decay of the BMRs via surface flux transport processes during the declining phase of the solar cycle (Babcock, 1961; Bhowmik & Nandy, 2018; Leighton, 1969). The large-scale solar magnetic field that is tied to the solar activity cycles as described above governs the coronal conditions and plays a role in balancing the heliospheric open flux and the resulting HMF (see e.g., Pal et al., 2020; Schwadron et al., 2010).

Many attempts have been made to understand the cause of the longer-term solar variations. These variations dictate the amplitude of the solar cycles (Hathaway, 2010; Hazra & Nandy, 2019; Hazra et al., 2014; Lockwood, 2001; Lockwood et al., 1999; Passos et al., 2014; Usoskin, 2013; Vaquero, 2016; Weiss & Tobias, 2016)

and thus affect space weather. As we are resuming human deep space explorations, there is an ever-growing need to investigate the possibility of entering a deep secular minimum in the coming decades.

Radiation from galactic cosmic rays (GCRs) is the main source of concern for crewed space missions. GCRs are energetic particles, consisting of protons, heavier ions, and a small fraction of electrons, which enter the heliosphere from the outer space. More than 90% of the GCRs are deflected at the interface between the heliosphere and the interstellar medium by the slowed solar wind. The residual GCRs that enter the heliosphere are modulated by the HMF. The flux of GCRs, which is inversely correlated with the HMF and solar activity (Schwadron et al., 2014; Usoskin, 2013), reaches its maximum during solar minimum, when the HMF is too weak to modulate GCRs effectively and vice versa. Their flux can be used to monitor variations of the solar activity, and thus ^{14}C and ^{10}Be radioisotopes, which are produced by the reaction of GCRs with the Earth's upper atmosphere, can provide a record of solar activity back to 10,000 years ago (Beer et al., 2011). The modulation of GCRs represents a response to the solar wind and the solar magnetic field over the scale of the entire heliosphere. GCR evolution, therefore, can uniquely reveal some of the trends we might not be able to see otherwise.

In a series of papers Lockwood (2010), Owens et al. (2011), and Barnard et al. (2011) investigated the statistical likelihood of a secular minimum, in particular, a Maunder-like grand minimum. They performed a superposed epoch analysis of the modulation parameter at the end of the previous grand solar maxima in the last 9300 years based on the composite reconstruction of the modulation parameter from Steinhilber et al. (2008). On the basis of past variations, the probability of a Maunder-like grand minimum in the coming 50 years was estimated to be around 1 in 12. Furthermore, Owens et al. (2017) created a data set for solar wind parameters dating back to 1617. They specifically investigated the Maunder minimum conditions to find the most probable coronal magnetic field configuration for this period (See Riley et al., 2015) so it could be used for any past or future grand minima.

Many researchers have attempted to predict the amplitude of the past four solar cycles (SC), 21–24 (1976–2020), using various methods (for a list of the models predicting SC24 and SC25, see Pesnell, 2012; Pesnell, 2016; Nandy, 2021, and the references therein). Pesnell (2016) concluded that more advanced models based on the solar magnetic field data are required to provide more reliable forecasts; predictions for SC24 showed a wide range of predicted amplitudes, proving that we are far from a consensus. Nandy (2021) argued that while there is no consensus on predicting the strength of SC25 among all existing studies, physics-based predictions have converged as a result of new insights of the solar dynamo.

Among the models investigated by Pesnell (2016); Nandy (2021), the most successful ones are based on the amplitude of the Sun's polar field (http://wso.stanford.edu/Polar.html) at previous solar minimum. These models predict a SC25 slightly weaker than SC24 (for example, Upton & Hathaway, 2018; Wang, 2017; Jiang et al., 2018). However, there are a few studies (based on the same methods) predicting SC25 to be somewhat more active than, although still comparable to the current cycle, for example, R. H. Cameron et al. (2016) and Bhowmik and Nandy (2018). Bhowmik and Nandy (2018) used models for the evolution of the Sun's surface and interior magnetic field and performed simulations of solar activity based on over a century of data. They provide a methodology that extends the prediction window to a decade (rather than the previous cycle minima).

McIntosh et al. (2020) and Leamon et al. (2020) have developed a methodology based on McIntosh et al. (2019) to find the terminator events indicative of the end of a cycle at the solar equator and the onset of a new cycle at mid-latitudes. Based on these terminators, McIntosh et al. (2020) and Leamon et al. (2020) predicted the onset of SC25 to be May 2020 (−1.5, +4 months) and that SC25 will be stronger than SC23 and SC24, which is in contrast with the predictions from the studies based on the amplitude of the Sun's polar field at solar minimum. In their analysis, they used activity bands that cancel out one another between the different polarization of two consecutive cycles when they co-exist. These activity bands explain why a prolonged solar minimum results in a weak next cycle. The solar Cycle 25 Prediction Panel (https://www.weather.gov/news/190504-sun-activity-in-solar-cycle) has gathered all these studies to predict the next cycle will peak at 95 to 130 averaged daily sunspot number. This prediction is most similar to the Gleissberg period (SC12-SC14) although there are still doubts about the length and amplitude of the next solar cycle.

The current study is motivated by the correlation observed between the HMF intensity and the modulation of GCRs reported by Rahmanifard et al. (2020) and Schwadron et al. (2014). After a brief discussion of the modulation potential (Section 2), in Section 3, we show that plotting these correlations for the past 24 cycles suggests we have moved to a modern secular minimum. In Section 4, we investigate these correlation plots and categorize the

observed trends to develop a tool to predict the subsequent cycles. Based on these trends, we show that SC25 will be as weak as or weaker than SC24. Throughout this paper, where we mention weaker (stronger) cycles, it refers to cycles with lower (higher) maximum HMF intensities than their previous cycles. Due to the well-established correlation between the sunspot number and HMF intensity, this can be roughly translated to weaker/stronger sunspot numbers, as well. In Section 5, we compare the previous secular minima to SC21-24 to gain more insight into how the next few solar cycles might proceed. A brief discussion and concluding remarks are provided in Sections 6 and 7.

2. Modulation of the GCRs in the Heliosphere

The flux of GCRs is presumed to be constant within the nearby interstellar medium on the timescales that we consider. However, recent studies provide more evidence that our solar system might be in the boundary region between interstellar clouds (Linsky et al., 2019). Passage of the solar system through a cloud with a 10-fold enhancement in the density with respect to the LISM will shrink the heliosphere by a factor of one-fourth (Zank & Frisch, 1999). This increases the flux of GCRs at 1 AU by 2–100 times for energetic protons between 10^3 – 10^2 MeV (Scherer et al., 2002). The solar wind pressure dropping due to successive weak cycles can also participate in the shrinkage of the heliosphere, leading to less effective modulation of the GCRs (Schwadron et al., 2011). Additionally, the large magnetic structures that filter GCRs at the edge of the heliosphere are accumulated over several solar cycles. Therefore, we expect this filtration to change with long-term solar variations (See Rahmanifard et al., 2020, for further discussion).

Inside the heliosphere, GCRs interact with the HMF across multiple scales. Hence, changes in the modulation of GCRs over the course of multiple cycles provide valuable information about the state of the heliosphere and reveal an underlying effect that would be difficult to ascertain by other means. This modulation, which is closely related to the HMF and thus solar activity as discussed in Section 1, is prone to the inherent randomness of solar activity. The effect of turbulent convection in the dispersion of the BMRs tilt, which is responsible for the birth of poloidal fields that initiate the next cycle, introduces randomness to the solar activity cycles and thus generates uncertainties in this analysis, which is based on the modulation of GCRs by the HMF.

The modulation of GCRs can be quantified by the so-called modulation potential adopted from the force field approximation of the Parker equation. The Badhwar-O'Neill 2014 model, hereafter BON14, provides a simplified version of the problem by solving stationary Fokker-Plank equations to transport the local interstellar spectrum of GCRs to 1 AU (O'Neill et al., 2015). The modulation potential, also known as the solar modulation parameter and deceleration potential, has a somewhat vague definition in the literature since it was first introduced by Gleeson and Axford (1968). It is defined as a quantity that approximately corresponds to the energy lost by GCR particles traveling from the LISM to the inner heliosphere and is related to the momentum per charge of the particles penetrating through the heliosphere. In the BON14 model, however, the modulation potential (ϕ) is an input parameter, which presents the level of modulation within their choice of parameters. Therefore, its absolute value is not significant; its variation with time is of greater importance. BON14 incorporates an ∼8–14 months delay through a function to find ϕ from sunspot number. In this way, they provide a time series of the modulation potential that extends back to 1750.

There are a few other models to find the intensity of GCRs, including Nymmik's model (Nymmik et al., 1996), which is a semi-empirical model similar to the BON14 model. Both these models describe GCR modulation through the heliosphere and thus provide invaluable knowledge about the structure of the heliosphere. BON2014 and Nymmik's model results are within 10% of each other, on average (Matthiä et al., 2013; de Wet, Slaba, Rahmanifard, Wislon, et al., 2020). Models similar to BON14 and Nymmik's model are appropriate for this type of analysis since they are based on the global sampling of GCRs calibrated to measurements near 1 AU. Alternatively, GCR fluxes can be used to find the characteristic modulation potential. CRaTER (Cosmic Ray Telescope for the Effect of Radiation, Spence et al., 2010) aims to investigate the radiation environment close to the lunar surface. The CRaTER instrument is designed to measure dose rates created by SEPs (solar energetic particles), GCRs, and other forms of radiation of lunar origin. de Wet et al. (2020) used the Monte Carlo N-Particle 6 (MCNP6) transport code to create a response function between the modulation potential values and CRaTER-observed dose rates from GCRs. They used various boundary condition fluxes associated with specific values of

modulation potential to provide a modulation potential data set based on the dose rates observed by the most shielded pair of detectors with a triple coincidence condition (de Wet, Slaba, Rahmanifard, Wilson, et al., 2020).

In our previous publication (Rahmanifard et al., 2020), we used CRaTER modulation potential data to investigate the correlation between the modulation potential and solar parameters for SC24. We adopted this method from Schwadron et al. (2014) to find a linear correlation between $< \phi > / < V >$ and $< B >$ in logarithmic space, where ϕ is the modulation potential from CRaTER data, V is the solar wind speed, and B is the magnitude of the HMF intensity. The <> symbol represents moving averages applied to data to eliminate the high-frequency variations and significant outliers (see Section 3 for more details). These studies were inspired by the power-law relation found by Schwadron et al. (2012) between the modulation potential (from Advanced Composition Explorer, ACE, data) and HMF, compatible with the slab turbulence of cosmic ray diffusion (le Roux et al., 1999).

The relationship between the modulation potential and the solar wind parameters has been examined in previous studies (Belov, 2000; Belov et al., 2001; Wibberenz & Cane, 2000; Wibberenz et al., 2002). Belov et al. (2001) used a contribution of several solar and heliospheric parameters including the current sheet tilt, polarity changes, and solar wind characteristics (the product of V_{SW} and $|B_{HMF}|$) in a semi-empirical model to predict GCR variations. They used this semi-empirical method to best describe the behavior of 10 GV GCRs intensity during SC20-SC22. The temporal variations of GCRs intensity at high energies can be described by propagating disturbance in the forcefield approximation and a continuous recovery process (Chih & Lee, 1986; Wibberenz & Cane, 2000; Wibberenz et al., 1998). Wibberenz et al. (2002) used this approximation to describe the GCRs depression as a function of $(V(t)/V_0)(B(t)/B_0)^n$ and used the observed intensity of GCRs for SC20-SC23 to show that $n \sim 1-2$ successfully predicts variations in GCRs intensity. Several other studies have found the value for n to be close to 2, which agrees well with Equation A6 from Schwadron et al. (2014) (le Roux et al., 1999; Zank et al., 1998; Burger et al., 2000). Schwadron et al. (2014) reported a correlation between modulation potential from ACE and CRaTER data, solar wind speed, and HMF intensity based on this equation. We updated this correlation for the entire cycle 24 to investigate the radiation environment in the coming solar cycle assuming a modern secular minimum (Rahmanifard et al., 2020). While the modulation potential from CRaTER (de Wet, Slaba, Rahmanifard, Wilson, et al., 2020) only covers SC24, this type of analysis can be extended to previous solar cycles using the BON14 modulation potential time series.

3. Correlation Plots Suggesting a Modern Secular Minimum

The hysteresis behavior observed for SC24 (Rahmanifard et al., 2020) motivated us to further investigate the correlation between the modulation potential from the BON14 model and solar wind parameters. Looking at these correlations reveals trends that can potentially be used to deduce the longer-term behavior of the Sun. Sunspot numbers are available for the last 24 cycles in monthly resolution, which makes possible the reconstruction of solar parameters and modulation potential for these cycles. We used HMF intensities from Rahmanifard et al. (2017) (for SC1-24, in monthly resolution where 7-month moving averages were applied), and the solar wind speed from Owens et al. (2017) (in yearly resolutions for <1973 and monthly resolution from 1973 onward with 7-month moving averages applied). For SC24, we used the most updated modulation values (monthly resolution) from CRaTER data (de Wet, Slaba, Rahmanifard, Wilson, et al., 2020), where they have applied 180-day moving averages. For SC1-23, we used the modulation parameter from BON14 (O'Neill et al., 2015) (in monthly values). We applied moving averages to the HMF strength and solar wind speed to eliminate the high-frequency variations and significant outliers so that the underlying patterns and trends could become visible. Modulation potential values from BON14 are smooth enough so that applying moving averages does not make any significant differences.

Adopting a color code to differentiate secular variations through the last 24 cycles reveals an interesting trend (Figure 1). Using light blue for cycles associated with previous secular minima (the Dalton, SC5-SC7 and the Gleissberg, SC12-SC14) and pink for all other cycles, which are mostly associated with secular maxima, creates two zones on the correlation plot. As can be seen, SC23 (red circles) falls in the secular maxima zone, as do the other cycles of the space age. However, the second half of SC23 moves toward the secular minima zone with a prolonged minimum connecting it to SC24. SC24, on the other hand, falls completely in the secular minima zone.

A pattern of a steep increase in the first half and a gentle decrease in the second half (most specifically in the last quarter) of SC24 seems to suggest another prolonged solar minimum leading to a weak SC25. Based

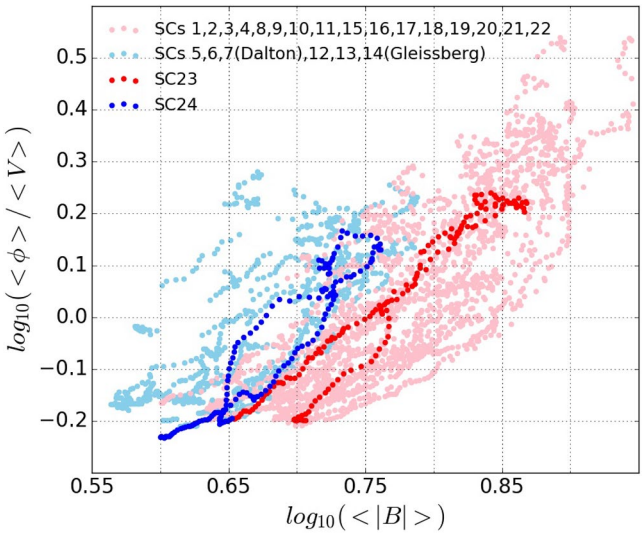

Figure 1. Correlation diagrams between $<\phi>/<V>$ and $<B>$ are shown in logarithmic space for the previous 24 solar cycles for which sunspot data is available. Cycles associated with secular maxima (minima) are shown in pink (light blue). SC23 and SC24 are shown in red and blue. It can be seen that at the end of cycle 23 we transited from the secular maxima zone to the secular minima zone.

on the correlation diagrams from the Dalton and the Gleissberg era (light blue circles), we expect SC25 and SC26 to stay in the secular minima zone and demonstrate activity levels below the average. Note that SC15 and SC16 (pink circles overlapping the blue minima) came at the end of the Gleissberg era and had lower than average solar activity. Additionally, while ϕ values vary with B, for the same value of B, ϕ values are different, depending on how weak or strong the cycles are. This creates two zones on the correlation plot that can distinguish cycles associated with secular minima from those associated with secular maxima.

4. Trends Observed in Previous Cycles

A closer look at previous cycles' correlation diagrams reveals trends that could be used to predict the subsequent cycles. In Figure 1, SC23 and SC24 demonstrate a steep increase in the first half and a gentle decrease in the second half, which might indicate a prolonged minimum and a weaker next cycle. Investigating these diagrams for the previous 24 solar cycles (Figure 2 and Figure 3) shows that these trends are observed through the past secular minima as well (see Section 5).

Investigating these diagrams for the past 24 solar cycles shows the converse trend also exists, where a gentle increase in the first half and a steep decrease in the second half is indicative of a stronger subsequent cycle (similar to SC7 in Figure 2). In addition, there are other possible forms, without as pronounced differences in the slopes between the two halves, leaving the next cycle inconclusive. These diagrams are presented in Figure 2, where Panel (a) shows odd cycles and Panel (b) shows even cycles. In this figure, the first (second) half of each cycle is shown with green (blue) data point. This makes it easy to see the sequence of time in these hysteretic diagrams.

The shapes of the correlation diagrams are different for odd and even cycles (Figure 2). After the magnetic field reversal in the solar maximum of even cycles ($A > 0$), the outward field lines in the northern pole cause positively charged ions such as GCR protons to drift down the poles. Therefore, these positive ions do not encounter irregularities in the current sheet or CMEs, which enhances their flux in the third quarter of even cycles and broadens their peak. Conversely, in odd cycles ($A < 0$), ions travel into the heliosphere along the current sheet, where irregularities convect them out (for example see Jokipii & Thomas, 1981; Webber & Lockwood, 1988). This leads to the distinctive alternate broad and sharp peaks in the flux of the GCRs, which in our correlation diagrams translate to hysteretic shapes for even cycles.

For odd cycles (Figure 2), it is quite straightforward to decide if a diagram is indicative of a weaker or stronger next cycle. If the first half of the cycle (green data points) falls below or more to the right (e.g., SC5), it can be indicative of a weaker next cycle and makes the shape of the diagram look like ↙. If the first half of odd cycles locates above or more to the left of the second half (blue data points), it can be indicative of a stronger next cycle (e.g., SC7) and has this shape ↗. For some of the cycles, this can be easily seen from the diagrams. However, for some other cycles, it can be very difficult to distinguish these trends since the two halves fall roughly on top of one another (↙). For these cycles (e.g., SC9), we can consider the diagram to be inconclusive.

We further developed a method to distinguish which half is located on the top of the other and to separate cycles that are inconclusive. To this end, we found the line correlated to the full solar cycle and defined the distance between the data points in the two halves in the space that is perpendicular to this correlated line (dashed black lines in Figure 2). For each data point in the first half, the length of these dashed black lines shows the distance from the second half. If the second half is on the top ($((<\phi_2>/<V_2>) > (<\phi_1>/<V_1>))$, this value is multiplied by -1.0. We found the averaged distance between the two halves for each cycle by averaging over all these values for all the data points in the first half, for which the dashed line intersects with the second half. If this averaged value is positive, the first half is on the top for most of the cycle, and we expect the next cycle to be stronger (SC1 and SC7). If this value is negative, the first half is on the bottom, and we expect the next cycle to be weaker (SC3, SC5, SC11, SC13, SC19, and SC23). If this value is close to zero (for cycles 9, 15, 17, 21,

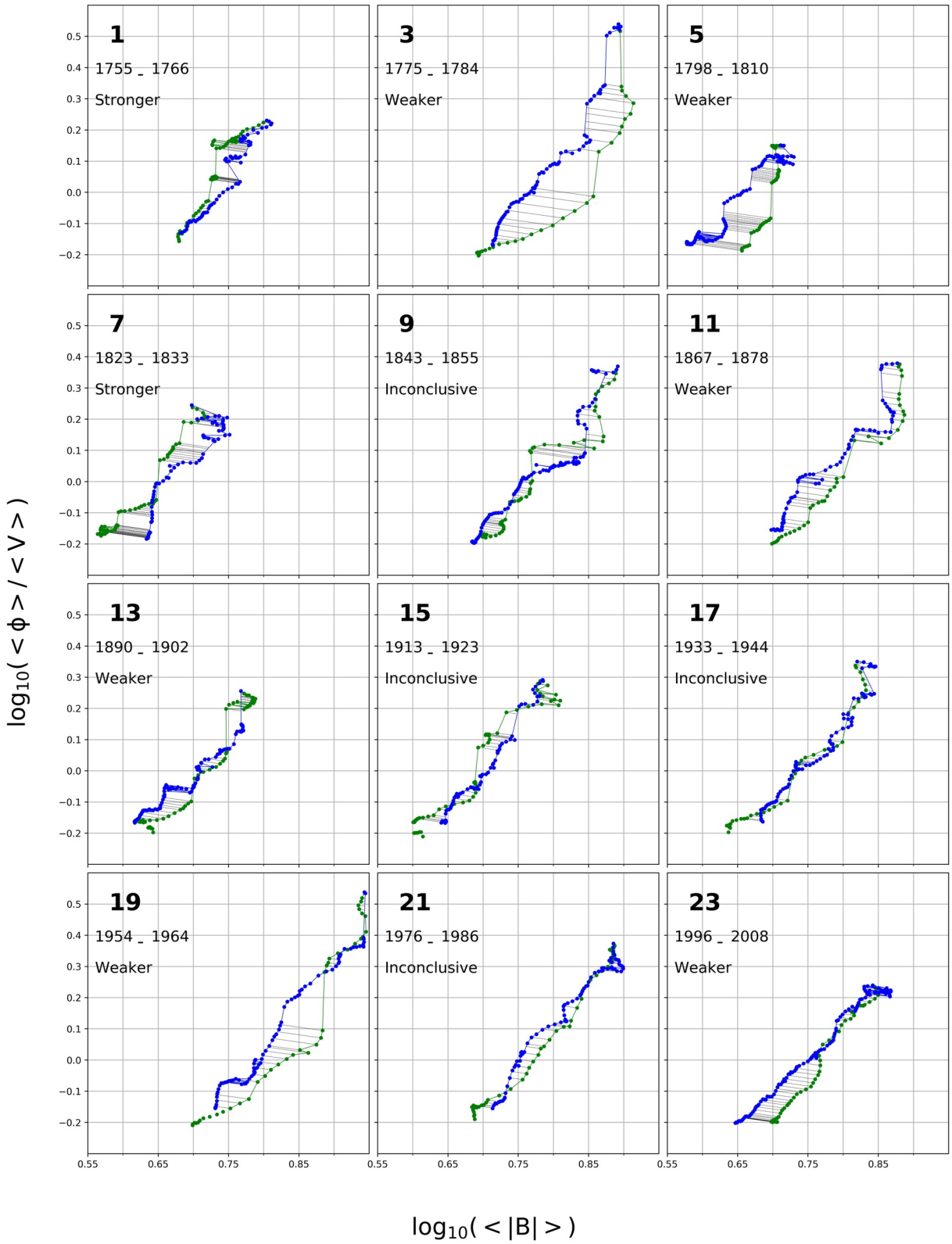

Figure 2. Correlation diagrams for odd cycles. Green data points represent the first half of cycles, and blue data points denote the second half of cycles. Dashed black lines that connect the two halves are used to find the distance between the two halves.

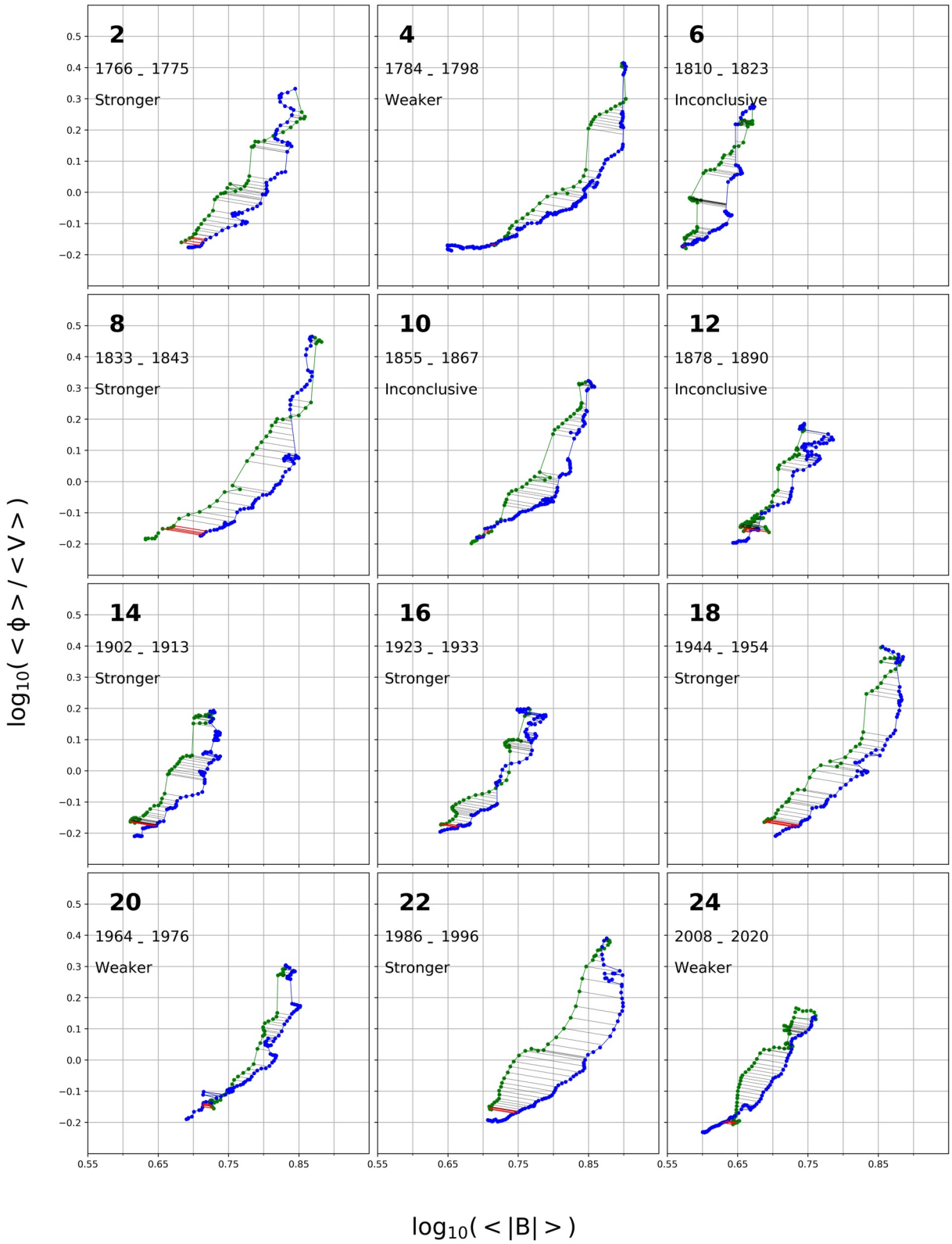

Figure 3. Correlation diagrams for even cycles. Green data points represent the first half of cycles, and blue data points denote the second half of cycles. Dashed black lines that connect the two halves are used to find the distance between the two halves. Red solid lines that connect the start of the two halves are used to determine if the cycle is open.

Table 1
The Averaged Distance Between the Two Halves for Odd Cycles

Solar Cycle	Averaged distance	Next cycle will be
1	0.024	Stronger
3	−0.050	Weaker
5	−0.039	Weaker
7	0.043	Stronger
9	−0.005	Inconclusive
11	−0.032	Weaker
13	−0.013	Weaker
15	0.006	Inconclusive
17	0.004	Inconclusive
19	−0.017	Weaker
21	−0.004	Inconclusive
23	−0.024	Weaker

the average of the distances are one order of magnitude smaller than the rest of the cycles), the next cycle remains inconclusive. Looking at the shape of these diagrams confirms the conclusions based on the numerical method. These averaged distances are gathered in Table 1. Diagrams associated with odd cycles are shown in Figure 2. Furthermore, the years of each solar cycle and our prediction for the next cycle are provided in Figure 2.

The enhancement of GCR's flux in the second half of even cycles, which translates to an abrupt decrease in modulation values, results in the distinctive hysteretic shape of even cycles. Therefore, in even cycles, the second half (blue data points) always falls on the right (below) of the correlation diagrams, which makes it challenging to find trends to predict the next cycle for them. To come up with a method to categorize the correlation diagrams, we used the criteria that if the loop is relatively open, like SC8 (), we consider this a cycle indicating a stronger next cycle. To decide if the shape of a diagram is open, we find the averaged distance between the two halves for each cycle (a) for the start of the cycle, 10% of the data points $\overline{D}_{start}$, shown in Figure 3 with solid red lines, and (b) for the full cycle ($\overline{D}_{full}$), dashed black lines. If the ratio $\overline{D}_{start}/\overline{D}_{full}$ is greater than 0.5, it means the diagram shape is relatively open, and we can consider the cycle to predict a stronger next cycle. These values are provided in Table 2, and the shape of the diagrams are shown in Figure 3. Based on these values and the diagrams from Figure 3, we expect SC2, SC8, SC14, SC16, SC18, and SC22 to predict a stronger next cycle.

However, for SC12, SC20, and SC24, while this ratio is significantly greater than 0.5, we can see from the shape of the diagrams that the cycle is definitely closed. This is because the tail of the second half after closing the cycle has extended in a way that the distance between the two halves is significant in comparison with the averaged distance for the full cycles (see Figure 3). In these cases, we trust that we can see the cycle is closed, and we consider them as closed cycles. If solar cycles with closed diagrams further extend their tail towards smaller $< B >$ values so that the data points are well passed the closing point (), this can be indicative of a prolonged solar minimum and predict a weaker next cycle. To find these cycles, we obtained the ratio between the length of the tail (second half data points with $< B >$ smaller than the minimum $< B >$ value for the first half data points) and the length of the full cycle (These values are provided in Table 2). SC4, SC20, and SC24 present a length ratio greater than 0.2 and thus predict a weaker next cycle. The remaining cycles (SC6, SC10, SC12) present a length ratio close to zero (, see Table 2) and thus are considered inconclusive about the next cycle. We have provided years of solar cycles and our predictions for even cycles in Figure 3.

Table 2
How Closed the Shape of the Cycle Is

Solar Cycle	Distance ratio (Start/full cycle)	Diagram is	Length ratio (Tail/full cycle)	Next cycle will be
2	0.802	Open		Stronger
4	0.142	Closed	0.231	Weaker
6	0.067	Closed	0	Inconclusive
8	1.862	Open		Stronger
10	0.239	Closed	0	Inconclusive
12	1.059	Closed by eye	0.045	Inconclusive
14	1.284	Open		Stronger
16	0.904	Open		Stronger
18	1.280	Open		Stronger
20	1.613	Closed by eye	0.264	Weaker
22	0.844	Open		Stronger
24	0.764	Closed by eye	0.221	Weaker

Our predictions for both odd and even cycles are listed in Table 3. As can be seen in this table, among the 16 cycles for which the shape of diagrams is conclusive, we can successfully predict whether the next cycle is stronger or weaker for 13 cycles. SC23 shows that SC24 would be a weaker cycle, which agrees with our observations. SC24 is also predicting the next cycle will be a weaker cycle (Figure 3). If this will be the case, we are probably entering an era of extreme decline in solar activity, similar to the Dalton and Gleissberg period.

Another look at the shapes presented in Table 3 might suggest that in most cases what dictates if the next cycle would be stronger (or weaker) than the current cycle is whether the cycle starts at lower (or higher) B values than it ends. This might be associated with a correlation between the strength of solar cycles and the minimum B values at the end of their previous cycles. This correlation has been previously examined in several studies (in terms of the SSN or polar magnetic field), for example, Brown (1976); Cameron and Schussler (2007); Du et al. (2008); Kane (2008); Muñoz-Jaramillo et al. (2013); Solanki et al. (2002); Vaquero and Trigo (2008); Wilson (1990);

Table 3
Predicting the Next Solar Cycle Based on the Correlation Diagrams

Trends Observed						
Cycle is	Odd	Even	Od	Even	Odd	Even
Next cycle will be	Weaker	Weaker	Stronger	Stronger	Inconclusive	Inconclusive
Cycle Numbers	3, 5, 11, 13, 19, 23	4, 20, 24	1, 7	2, 8, 14, 16, 18,22	9, 15,17, 21	6, 10, 12,
Our prediction is	✓, ✓, ✓	✓, X, ?	✓, ✓	✓, X, ✓		
Correct (✓)/incorrect (X)	✓, ✓, ✓			✓, ✓, X		

Yoshida (2014). We have shown this correlation in Figure 4, by presenting B_{Min} observed at the end of each cycle versus the B_{Max} associated with the next cycle (based on reconstructed values of the HMF intensity from Rahmanifard et al., 2017). The black line in this figure shows the correlation with a correlation coefficient of 0.74 and a p-value of 0.000 05. The gray shaded area shows the uncertainty region at 95% confidence interval. While data points are shown with gray circles, blue (or red) "x" signs mark cycles that are predicted to be weaker (or stronger) than their previous cycles based on Table 3. Blue squares (or green triangles) enclose gray circles for cycles associated with the Dalton (or Gleissberg) period.

As can be seen in Figure 4, cycles that are predicted to be weaker (gray circles with blue x) are mostly concentrated below the correlation line, cycles that are predicted to be stronger (gray circles with red x) have concentrated above the correlation line, and cycles that remain inconclusive (gray circles) are the most aligned with the correlation fit. Hence, excluding the data points associated with a weaker or stronger next cycle improves the correlation coefficient significantly ($R = 0.95$ and a $p = 0.0009$). This suggests that on top of the well-established correlation between B_{Min} and cycle strength, our analysis provides additional information for predicting cycle strength. This additional information is probably reliant on the steps that connects the GCRs modulation to solar activity.

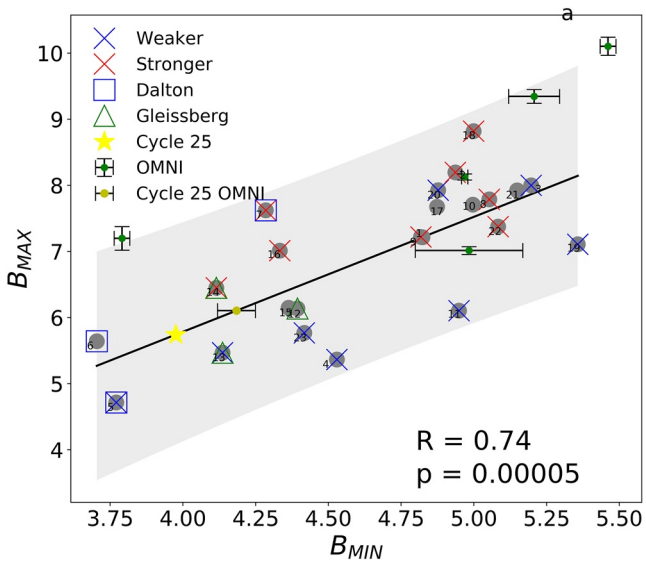

Figure 4. B_{Max} versus B_{Min} at the end of the previous cycle. The black line shows the correlation with a correlation coefficient of ~0.74 and a p-value of 0.000 05. Gray shaded area represents uncertainty with 95% confidence level. Gray circles represent data points for each cycle, and blue (or red) x signs mark cycles that are predicted to be weaker (or stronger) than their previous cycles. Considering only the inconclusive cycles provides a better correlation ($R = 0.95$ and $p = 0.0009$). Blue (or green) squares (or triangles) enclose cycles associated with the Dalton (or Gleissberg) period. Green circles with error bars represent datapoints from OMNI data set. The yellow star (circle with error bar) shows our prediction for SC25 based on SC24 B_{Min} from Rahmanifard (2017) (or OMNI data).

The HMF values used in this study are obtained from Rahmanifard et al. (2017) model. This model provides a historical record for HMF values using timescales associated with the processes involved in the balance of the heliospheric magnetic flux. It also uses sunspot numbers as a proxy for the closed magnetic flux introduced to this balance throughout the previous 24 cycles. This model presents fairly good agreement with geomagnetic data as well as OMNI data. However, there are still differences between this model predictions and OMNI data, particularly in extremums. We have added datapoints from OMNI data (green circles with error bars, showing 95% confidence interval) to Figure 4 to show that in spite of differences they still agree within uncertainties.

Using $B_{\mathrm{Min}} = 3.98$ nT, obtained for May 2020 from Rahmanifard et al. (2017) model, we find SC25 B_{Max} to be $\sim 5.74 \pm 0.80$ (shown with a yellow star), which is similar to SC24 ($B_{\mathrm{Max}} = 5.77$ nT). This makes these two cycles the weakest since SC14 ($B_{\mathrm{Max}} = 5.47$ nT). Using $B_{\mathrm{Min}} = 4.18 \pm 0.03$ nT from OMNI data (yellow circle with 95% confidence error bar) obtains $\sim 6.10 \pm 0.91$ for B_{Max}, which agrees with the prediction obtained based on Rahmanifard et al. (2017) model results within uncertainties. The predicted intensity of $B_{\mathrm{Max}} = 5.74 \pm 0.80$ nT, or the 6.10 ± 0.91 value based on OMNI data, for SC25, is consistent with the amplitude of 95–130 averaged daily sunspot number as the consensus statement reported by the Solar Cycle 25 Prediction Panel

(https://www.weather.gov/news/190504-sun-activity-in-solar-cycle). Moreover, it would constitute an SC25 slightly weaker than SC13 ($B_{\mathrm{Max}} = 6.14$ nT) in the Gleissberg era, although still stronger than SC6 ($B_{\mathrm{Max}} = 4.72$ nT) in the

Dalton era. While both these values present below-average solar activity, it must be noted that based on the trends found in this study they likely overestimate the strength on SC25.

5. Previous Secular Minima Versus a Modern Secular Minimum

Looking at correlation diagrams associated with the Dalton and the Gleissberg minima provides more insight into how the next few solar cycles might proceed. The Dalton minimum period covered SC5-SC7 (1790–1830), and it contains the weakest recorded solar activity since routine monthly sunspot numbers became available. In Figure 5a, we show SC4 to SC8 to demonstrate how cycles move to and from the secular minima zone. We have shown each cycle with a different color, with the beginning of each cycle being the darkest and the end of the cycle being the lightest. As can be seen, a shallow slope in the last quarter of SC4 (green data points) leads to a weak SC5 (red). The same trend persists for SC5 (red) leading to a weak SC6. The shape of SC6 (blue) remains inconclusive (based on the trends introduced in Table 3) and leads to a SC7(gray) which contains higher B. Finally, SC7 breaks the trend by showing a steep slope in its last quarter, leading to a stronger SC8 (purple), ending the secular minimum.

The next secular minimum, the Gleissberg period (SC12-SC14), is shown in Figure 5b. In this figure, we again applied different colors for each cycle, with the darkest data point denoting the beginning and the lightest denoting the end of cycles. The same trend–though not as pronounced as in the Dalton period–of a gradual decrease in $< \phi >/< V >$ in the last phases of these cycles leads to weak cycles one after another to form a secular minimum.

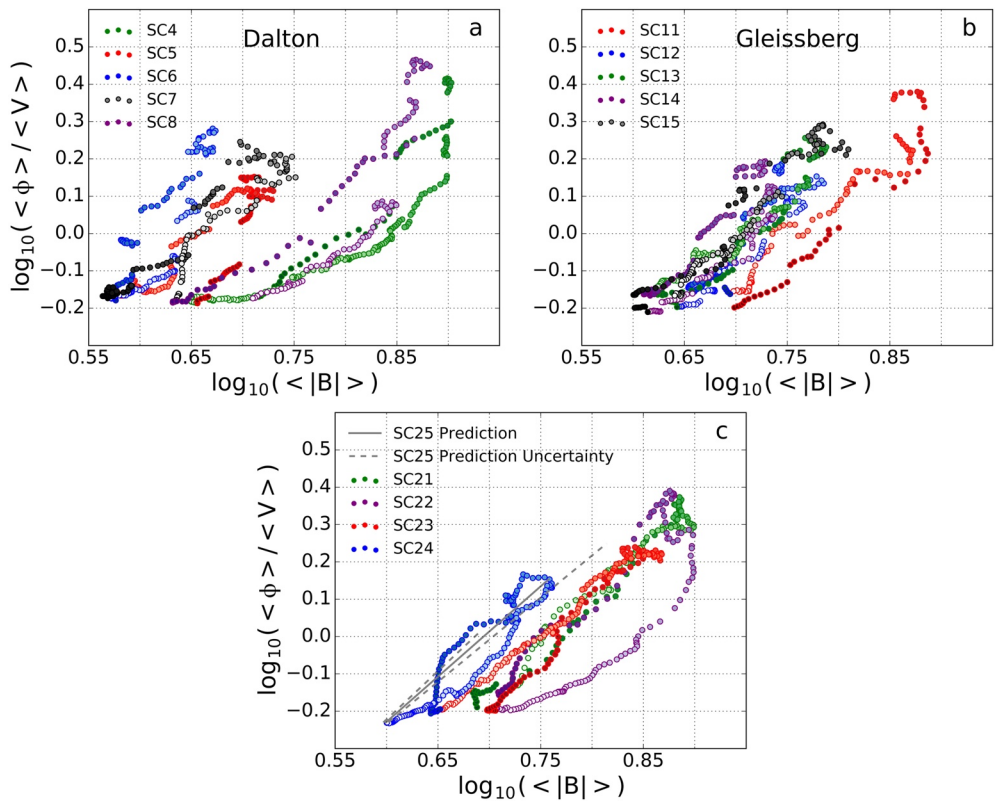

Figure 5. Panels a, b, and c show the correlation diagrams for the Dalton, the Gleissberg, and modern era. In panel a, in addition to SC5 to SC7, we have included SC4 and SC8 to show how the transit occurs to and from a secular minimum. In the same way, in panel b, we have shown the transit from SC11 to SC12 through SC15, for the Gleissberg period. In panel c, we have shown the SC21 through SC24, with SC24 seeming to be the first cycle of a modern secular/grand minimum. In panel c, n addition to SC21-SC24 our prediction for SC25 is shown based on a prediction of $B_{Max} = 5.74 \pm 0.80$ from panel a using gray solid line. Gray dashed lines represent uncertainty.

In Figure 5c, we show SC24 to compare it with the Dalton and Gleissberg cycles presented in panels a and b. While the shape of the correlation diagram is inconclusive for SC21 and SC22, a gradual decrease at the end of SC23 leads SC24 to reside in the secular minima zone. SC23 shows that SC24 would be a weaker cycle, which agrees with our observations. SC24 is also predicting the next cycle will be a weaker cycle.

The last data points of SC24 (associated with May 2020, in light blue) represent modulation potential values below the predicted floor by the BON14 model, which likely is indicative of the start of SC25 (for further explanations see Rahmanifard et al., 2020). This is in agreement with (Leamon et al., 2020), who estimated the onset of SC25 would be in May 2020, $-1.5 + 4$ months. However, Leamon et al. (2020) used a method based on terminator events (McIntosh et al., 2019) and predicted that SC25 will be significantly stronger than SC23 and SC24, which is contrast with our prediction of SC25. Starting from the observed point for May 2020, using a weighted average over the previous secular minima cycles for the slope and using $B_{\mathrm{Max}} = 5.74 \pm 0.80$ nT from Figure 4, we found a predicted linear correlation for SC25, gray solid line with gray dashed lines presenting the uncertainty region in Figure 5c. This uncertainty region represents our predicted SC25, $-1.5 + 4$ months uncertainty for the onset of SC25 along with our predicted uncertainty for SC25 B_{Max}. A more prolonged solar minimum will likely result in further decrease in B_{Min} at the end of SC24 resulting in a weaker SC25.

The prediction of $B_{\mathrm{Max}} = 5.74 \pm 0.80$ nT from Figure 4 demonstrates an SC25 slightly weaker than SC13 ($B_{\mathrm{Max}} = 6.14$ nT) in the Gleissberg era, although still stronger than SC6 ($B_{\mathrm{Max}} = 4.72$ nT) in the Dalton era. However, it is important to note that based on the trends found in this study the B_{Max} value used here likely overestimates the strength on SC25 (Section 4). The correlation plots and the radiation environment resulting from a Gleissberg-like and a Dalton-like SC25 were investigated in Rahmanifard et al. (2020). In a future study, we will investigate the radiation environment based on the correlation predicted here (Figure 5c).

6. Discussion

Correlations between the modulation potential values, solar wind speed, and the intensity of the HMF presented in this paper suggest that we are within a secular minimum, and are further used to deduce trends to predict solar activity. The obtained correlation diagrams and any further conclusions based on their shapes are obviously reliant on the accuracy of the inferred parameters employed in this study.

In Figure 1, we showed that plotting all the correlation diagrams in the last 24 solar cycles creates two distinctive zones associated with secular minima and maxima. Furthermore, we can see that in the last 23 solar cycles these diagrams have shifted to the secular minima zone only twice (the Dalton and the Gleissberg minima) and once more in the beginning of SC24. This suggests that we are currently in a secular minimum similar to the Dalton and the Gleissberg minima. This also means that the observed decline in solar activity will likely persist for another two solar cycles since both Dalton and Gleissberg minima were at least three solar cycles long. Therefore, we expect to see SC25 and SC26 stay in the secular minima zone and exhibit activity levels below the average.

Trends reported in this paper provide a way to predict the next solar cycle during the last phases of the current cycle. We showed that a steep increase in the first half and a gentle decrease in the second half of the correlation diagrams presented here can be indicative of a prolonged minimum leading to a weaker next cycle, while the opposite trend indicates the next cycle stronger than the current cycle. Based on the correlation presented in Figure 4 between the maximum HMF intensity of a cycle (B_{Max}) and the minimum HMF observed for the previous cycle (B_{Min}), we found that cycles that are predicted to be weaker (based on the trends found here) mostly demonstrate values lower than predicted by this correlation and cycles that are predicted to be stronger present larger values. This suggests that the correlation diagrams reveal a physical effect in addition to the correlation between B_{Min} and B_{Max}. Although odd cycles have historically shown to be stronger than their adjacent even cycles (Gnevyshev & Ohl, 1948), the small slope at the end of SC24 suggests that SC25 will be a weaker cycle than SC24. Therefore, while, based on Figure 4, SC25 is predicted to be as weak as SC24 with $B_{\mathrm{Max}} = 5.74 \pm 0.80$, this value likely overestimates the strength of SC25.

The correlation diagrams correctly predict 13 cycles out of the 16 cycles for which these trends have been observed. This means that in ~70% of cycles, where a prediction is possible, it correctly predicts whether the subsequent cycle will be weaker or stronger in ~81% of the cases. The seven cycles (30%) that remain inconclusive manifest a significant correlation between the maximum HMF intensity and the minimum HMF observed for the

previous cycle. Therefore, the diagrams presented in this study along with the B_{Min} versus B_{Max} correlation for the inconclusive cycles form a tool to predict the strength of the next solar cycle at the end of the current cycle.

The modern secular minimum that we are experiencing will substantially affect our space radiation environment, and therefore future space missions. During the weak cycles that are awaiting us, solar maximum is safer for long-term space exploration due to more effective modulation of GCRs, provided that very large SEP events are infrequent. While SEP events are expected to be more frequent during solar maximum, a weak SC25 as predicted in this study will make such events scarcer than before. However, to protect the crew against radiation hazards caused by events such as the September 2017 event (Schwadron et al., 2018), real-time monitoring of solar events would be essential. The effect of these new conditions on the lunar radiation environment and explorations is yet to be understood (Looper et al., 2013; Spence et al., 2013).

A modern secular minimum would provide an exceptional opportunity to investigate our interstellar environment in the absence of extreme solar events. These years of unprecedentedly low solar activity provide a rare chance to study components of the interstellar medium that enter the heliosphere such as GCRs, the interstellar neutrals, and energetic neutral atoms with the interstellar origin. IBEX (Interstellar Boundary Explorer, McComas et al., 2009) measurements have already provided valuable data through SC24. Selected for launch in 2024, IMAP (Interstellar Mapping and Acceleration Probe, McComas et al., 2018) will further investigate the interaction between the heliosphere and the very local interstellar medium.

7. Conclusion

A persistent decline of the solar activity level, at the end of the space age secular maximum, indicates the possibility that the Sun has already entered a secular solar minimum. In this paper, we used the correlation between the modulation potential and solar wind parameters to show that indeed we are in a secular minimum. We used trends observed in the correlation diagrams of the last 24 solar cycles to find a way to predict subsequent solar cycle during the last phases of the current cycle. Using this method, we predict SC25 to be as weak as or weaker than SC24 ($B_{Max} = 5.74 \pm 0.80$). Based on the historical records, if the Sun repeats the same trends observed for the Dalton and Gleissberg secular minima, we expect SC26 to be weak.

Data Availability Statement

All datasets are available at https://crater-web.sr.unh.edu/Rahmanifard2021.

Acknowledgment
This work was supported by NASA SSERVI LEADER (grant number 80NSSC20M0021) and CRaTER, LRO program (contract number NNG11PA03C).

References

Abreu, J. A., Beer, J., Steinhilber, F., Tobias, S. M., & Weiss, N. O. (2008). For how long will the current grand maximum of solar activity persist? *Geophysical Research Letters*, *35*(20). https://doi.org/10.1029/2008GL035442

Babcock, H. W. (1961). The topology of the Sun's magnetic field and the 22-year cycle. The *Astrophysical Journal*, *133*, 572. https://doi.org/10.1086/147060

Barnard, L., Lockwood, M., Hapgood, M. A., Owens, M. J., Davis, C. J., & Steinhilber, F. (2011). Predicting space climate change. *Geophysical Research Letters*, *38*(16), L16103. https://doi.org/10.1029/2011GL048489

Beer, J., McCracken, K. G., Abreu, J., Heikkilä, U., & Steinhilber, F. (2011). Cosmogenic radionuclides as an extension of the neutron monitor era into the past: Potential and limitations. *Space Science Reviews*, *176*(1–4), 89–100. https://doi.org/10.1007/s11214-011-9843-3

Belov, A. (2000). Large scale modulation: View from the Earth. In K. R. Bieber, E. Eroshenko, P. Evenson, & E. O. Flückiger (Eds.), *Cosmic rays and earth* (pp. 79–105). Springer. https://doi.org/10.1007/978-94-017-1187-6_5

Belov, A., Gushchina, R., Obridko, V., Shelting, B., & Yanke, V. (2001). International conference on cosmic rays. In *Long-term variations of galactic cosmic rays and their relation to the solar magnetic field parameters* (pp. 3911–3914). Retrieved from http://adsabs.harvard.edu/pdf/2001ICRC\\ldots10.3911B

Bhowmik, P., & Nandy, D. (2018). Prediction of the strength and timing of sunspot cycle 25 reveal decadal-scale space environmental conditions. *Nature Communications*, *9*(1). https://doi.org/10.1038/s41467-018-07690-0

Brown, G. M. (1976). What determines sunspot maximum? *Monthly Notices of the Royal Astronomical Society*, *174*, 185–189. https://doi.org/10.1093/mnras/174.1.185

Burger, R. A., Potgieter, M. S., & Heber, B. (2000). Rigidity dependence of cosmic ray proton latitudinal gradients measured by the Ulysses spacecraft' Implications for the diffusion tensor. *Journal of Geophysical Research*, *105*(27), 447–27455. https://doi.org/10.1029/2000JA000153

Cameron, R., & Schussler, M. (2007). Solar cycle prediction using precursors and flux transport models. *The Astrophysical Journal*, *659*(1), 801–811. https://doi.org/10.1086/512049

Cameron, R. H., Jiang, J., & Schuessler, M. (2016). Solar cycle 25: Another moderate cycle? *The Astrophysical Journal Letters*, *823*(22), 5. https://doi.org/10.3847/2041-8205/823/2/L22

Charbonneau, P. (2010). Dynamo models of the solar cycle. *Living Reviews in Solar Physics*, *2*(1), 1–83. https://doi.org/10.12942/lrsp-2005-2

Chih, P. P., & Lee, M. A. (1986). A perturbation approach to cosmic ray transients in interplanetary space. *Journal of Geophysical Research*, *91*(A3), 2903–2913. https://doi.org/10.1029/ja091ia03p02903

de Wet, W. C., Slaba, T. C., Rahmanifard, F., Wilson, J. K., Jordan, A. P., Townsend, L. W., et al. (2020). CRaTER observations and permissible mission duration for human operations in deep space. *Life Sciences in Space Research*, *26*(December 2019), 149–162. https://doi.org/10.1016/j.lssr.2020.04.004

Du, Z. L., Wang, H. N., & Zhang, L. Y. (2008). A running average method for predicting the size and length of a solar cycle. *Chinese Journal of Astronomy and Astrophysics*, *8*(4), 477–488. https://doi.org/10.1088/1009-9271/8/4/12

Gleeson, L. J., & Axford, W. I. (1968). Solar modulation of galactic cosmic rays. *The Astrophysical Journal*, *154*, 1011. https://doi.org/10.1086/149822

Gnevyshev, M., & Ohl, A. (1948). On the 22-year cycle of solar activity. *Astronomiceskij Zurnal*, *25*, 18–20.

Hathaway, D. H. (2010). The solar cycle imprint/terms of use. *Living Reviews in Solar Physics*, *7*(1), 1–65. https://doi.org/10.12942/lrsp-2010-1

Hazra, S., & Nandy, D. (2019). The origin of parity changes in the solar cycle. *Monthly Notices of the Royal Astronomical Society*, *489*(3), 4329–4337. https://doi.org/10.1093/mnras/stz2476

Hazra, S., Passos, D., & Nandy, D. (2014). A stochastically forced time delay solar dynamo model: Self-consistent recovery from a maunder-like grand minimum necessitates a mean-field alpha effect. *The Astrophysical Journal*, *789*(1), 5. https://doi.org/10.1088/0004-637X/789/1/5

Jiang, J., Wang, J. X., Jiao, Q. R., & Cao, J. B. (2018). Predictability of the Solar Cycle Over One Cycle. *The Astrophysical Journal*, *863*(2), 159. https://doi.org/10.3847/1538-4357/aad197

Jokipii, J. R., & Thomas, B. (1981). Effects of drift on the transport of cosmic rays IV. Modulation by a wavy interplanetary current sheet J. *The Astrophysical Journal*, *243*, 1115–1122. https://doi.org/10.1086/158675

Kane, R. P. (2008). Prediction of solar cycle maximum using solar cycle lengths. *Solar Physics*, *248*(1), 203–209. https://doi.org/10.1007/s11207-008-9125-8

Leamon, R. J., McIntosh, S. W., Chapman, S. C., & Watkins, N. W. (2020). Timing terminators: Forecasting sunspot cycle 25 onset. *Solar Physics*, *295*(2), 1–18. https://doi.org/10.1007/s11207-020-1595-3

Leighton, R. B. (1969). A Magneto-Kinematic Model of the Solar Cycle. The *Astrophysical Journal*, *156*(April), 1. https://doi.org/10.1086/149943

le Roux, J. A., Zank, G. P., & Ptuskin, V. S. (1999). An evaluation of perpendicular diffusion models regarding cosmic ray modulation on the basis of a hydromagnetic description for solar wind turbulence. *Journal of Geophysical Research: Space Physics*, *104*(A11), 24845–24862. https://doi.org/10.1029/1999ja900318

Linsky, J. L., Redfield, S., & Tilipman, D. (2019). *The interface between the outer heliosphere and the inner Lism: Morphology of the Local interstellar cloud, its hydrogen hole, Stromgren Shells, and 60Fe accretion*. arXiv (Vol. 886, p. 41). https://doi.org/10.3847/1538-4357/ab498a

Lockwood, M. (2001). Long-term variations in the magnetic fields of the Sun and the heliosphere: Their origin, effects, and implications. *Journal of Geophysical Research: Space Physics*, *106*(A8), 16021–16038. https://doi.org/10.1029/2000ja000115

Lockwood, M. (2010). Solar change and climate: An update in the light of the current exceptional solar minimum. *Proceedings of the Royal Society A: Mathematical, Physical & Engineering Sciences*, *466*(2114), 303–329. https://doi.org/10.1098/rspa.2009.0519

Lockwood, M., Stamper, R., & Wild, M. N. (1999). A doubling of the Sun's coronal magnetic field during the past 100 years. *Nature*, *399*(6735), 437–439. https://doi.org/10.1038/20867

Looper, M. D., Mazur, J. E., Blake, J. B., Spence, H. E., Schwadron, N. A., Golightly, M. J., et al. (2013). The radiation environment near the lunar surface: CRaTER observations and Geant4 simulations. *Space Weather*, *11*(4), 142–152. https://doi.org/10.1002/swe.20034

Matthiä, D., Berger, T., Mrigakshi, A. I., & Reitz, G. (2013). A ready-to-use galactic cosmic ray model. *Advances in Space Research*, *51*(3), 329–338. https://doi.org/10.1016/j.asr.2012.09.022

McComas, D. J., Allegrini, F., Bochsler, P., Bzowski, M., Christian, E. R., Crew, G. B., et al. (2009). Global observations of the interstellar interaction from the Interstellar Boundary Explorer (IBEX). *Science*, *326*(5955), 959–962. https://doi.org/10.1126/science.1180906

McComas, D. J., Christian, E. R., Schwadron, N. A., Fox, N., Westlake, J., Allegrini, F., et al. (2018). Interstellar Mapping and Acceleration Probe (IMAP): A New NASA Mission. *Space Science Reviews*, *214*(8), 116. https://doi.org/10.1007/s11214-018-0550-1

McIntosh, S. W., Chapman, S., Leamon, R. J., Egeland, R., & Watkins, N. W. (2020). Overlapping magnetic activity cycles and the sunspot number: Forecasting sunspot cycle 25 amplitude. *Solar Physics*, *295*(12). https://doi.org/10.1007/s11207-020-01723-y

McIntosh, S. W., Leamon, R. J., Egeland, R., Dikpati, M., Fan, Y., & Rempel, M. (2019). What the Sudden death of solar cycles can tell us about the nature of the solar interior. *Solar Physics*, *294*(7). https://doi.org/10.1007/s11207-019-1474-y

Muñoz-Jaramillo, A., Dasi-Espuig, M., Balmaceda, L. A., & Deluca, E. E. (2013). Solar cycle propagation, memory, and prediction: Insights from a century of magnetic proxies. The *Astrophysical Journal Letters*, *767*(2), L25. https://doi.org/10.1088/2041-8205/767/2/L25

Nandy, D. (2021). Progress in solar cycle predictions: Sunspot cycles 24–25 in perspective: Invited review. *Solar Physics*, *296*(3). https://doi.org/10.1007/s11207-021-01797-2

Nymmik, R. A., Panasyuk, M. I., & Suslov, A. A. (1996). No TitleGalactic cosmic ray flux simulation and prediction. *Advances in Space Research*, *17*(2), 19–30. https://doi.org/10.1016/0273-1177(95)00508-C

O'Neill, P. M., Golge, S., & Slaba, T. C. (2015). *NASA-TP-2015-218569-Badhwar-O'Neill 2014 galactic cosmic ray flux model description (Technical Report No. March)*. NASA Johnson Space Center. Retrieved from https://ntrs.nasa.gov/search.jsp?R=20150003026

Owens, M. J., Lockwood, M., Barnard, L., & Davis, C. J. (2011). Solar cycle 24: Implications for energetic particles and long-term space climate change. *Geophysical Research Letters*, *38*(19), L19106. https://doi.org/10.1029/2011GL049328

Owens, M. J., Lockwood, M., & Riley, P. (2017). Global solar wind variations over the last four centuries. *Nature Publishing Group*, *7*(January), 1–11. https://doi.org/10.1038/srep41548

Pal, S., Dash, S., & Nandy, D. (2020). Flux erosion of magnetic clouds by reconnection with the Sun's open flux. *Geophysical Research Letters*, *47*(8), 1–10. https://doi.org/10.1029/2019GL086372

Passos, D., Nandy, D., Hazra, S., & Lopes, I. (2014). A solar dynamo model driven by mean-field alpha and Babcock-Leighton sources: Fluctuations, grand-minima-maxima, and hemispheric asymmetry in sunspot cycles. *Astronomy and Astrophysics*, *563*, 1–9. https://doi.org/10.1051/0004-6361/201322635

Pesnell, W. D. (2012). Solar cycle predictions (invited review). *Solar Physics*, *281*(1), 507–532. https://doi.org/10.1007/s11207-012-9997-5

Pesnell, W. D. (2016). Predictions of Solar Cycle 24: How are we doing? *Space Weather*, *14*(1), 10–21. https://doi.org/10.1002/2015SW001304

Rahmanifard, F., de Wet, W. C., Schwadron, N. A., Owens, M. J., Jordan, A. P., Wilson, J. K., et al. (2020). Galactic cosmic radiation in the interplanetary space through a modern secular minimum. *Space Weather*, *18*(9). https://doi.org/10.1029/2019SW002428

Rahmanifard, F., Schwadron, N. A., Smith, C. W., McCracken, K. G., Duderstadt, K. A., Lugaz, N., & Goelzer, M. L. (2017). Inferring the heliospheric magnetic field back through Maunder Minimum. *The Astrophysical Journal*, *837*(2), 165. https://doi.org/10.3847/1538-4357/aa6191

Riley, P., Lionello, R., Linker, J. A., Cliver, E., Balogh, A., Beer, J., et al. (2015). Inferring the structure of the solar corona and inner heliosphere during the maunder minimum using global thermodynamic magnetohydrodynamic simulations. *The Astrophysical Journal*, *802*(2), 105. https://doi.org/10.1088/0004-637X/802/2/105

Scherer, K., Fichtner, H., & Stawicki, O. (2002). Shielded by the wind: The influence of the interstellar medium on the environment of Earth. *Journal of Atmospheric and Solar-Terrestrial Physics*, *64*(7), 795–804. https://doi.org/10.1016/S1364-6826(02)00078-0

Schwadron, N. A., Baker, T., Blake, B., Case, A. W., Cooper, J. F., Golightly, M., et al. (2012). Lunar radiation environment and space weathering from the Cosmic Ray Telescope for the Effects of Radiation (CRaTER). *Journal of Geophysical Research E: Planets*, *117*(3), E00H13. https://doi.org/10.1029/2011JE003978

Schwadron, N. A., Blake, J. B., Case, A. W., Joyce, C. J., Kasper, J., Mazur, J., et al. (2014). Special section : Does the worsening galactic cosmic radiation environment observed by CRaTER preclude future manned deep space exploration. *Space Weather*, *12*(11), 622–632. https://doi.org/10.1002/2014SW001084

Schwadron, N. A., Connick, D. E., & Smith, C. W. (2010). Magnetic flux balance in the heliosphere. *The Astrophysical Journal*, *722*(September), 132–L136. https://doi.org/10.1088/2041-8205/722/2/L132

Schwadron, N. A., Rahmanifard, F., Wilson, J., Jordan, A. P., Spence, H. E., Joyce, C. J., et al. (2018). Update on the Worsening particle radiation environment observed by CRaTER and implications for future human deep-space exploration. *Space Weather*, *16*, 289–303. https://doi.org/10.1002/2017sw001803

Schwadron, N. A., Spence, H. E., & Came, R. (2011). Does the space environment affect the ecosphere? *Eos*, *92*(36), 297–298. https://doi.org/10.1029/2011EO360001

Solanki, S. K., Schüssler, M., & Fligge, M. (2002). Secular variation of the Sun's magnetic flux. *Astronomy and Astrophysics*, *383*, 706–712. https://doi.org/10.1051/0004-6361:20011790

Spence, H. E., Case, A. W., Golightly, M. J., Heine, T., Larsen, B. A., Blake, J. B., et al. (2010). CRaTER: The cosmic ray telescope for the effects of radiation experiment on the lunar reconnaissance orbiter mission. *Space Science Reviews*, *150*(1–4), 243–284. https://doi.org/10.1007/s11214-009-9584-8

Spence, H. E., Golightly, M. J., Joyce, C. J., Looper, M. D., Schwadron, N. A., Smith, S. S., et al. (2013). Relative contributions of galactic cosmic rays and lunar proton "albedo" to dose and dose rates near the Moon. *Space Weather*, *11*(11), 643–650. https://doi.org/10.1002/2013SW000995

Steinhilber, F., Abreu, J. A., & Beer, J. (2008). Solar modulation during the Holocene. *Astrophysics and Space Sciences Transactions*, *4*(1), 1–6. https://doi.org/10.5194/astra-4-1-2008

Upton, L. A., & Hathaway, D. H. (2018). An updated solar cycle 25 prediction with AFT: The modern minimum. *Geophysical Research Letters*, *45*(16), 8091–8095. https://doi.org/10.1029/2018GL078387

Usoskin, I. G. (2013). A history of solar activity over millennia. *Living Reviews in Solar Physics*, *10*(1), 1–88. https://doi.org/10.12942/lrsp-2013-1

Vaquero, J. M. (2016). Long-term variation of solar activity: Recent progress. In S. P.-H. S. Arribas, A. Alonso-Herrero, F. Figueras, C. Hernández-Monteagudo, & A. Sánchez-Lavega (Eds.), *Scientific meeting of the Spanish astronomical society. Bilbao, Spain*. Retrieved from https://ui.adsabs.harvard.edu/abs/2017hsa9.conf.579V/abstract

Vaquero, J. M., & Trigo, R. M. (2008). Can the solar cycle amplitude be predicted using the preceding solar cycle length? *Solar Physics*, *250*(1), 199–206. https://doi.org/10.1007/s11207-008-9211-y

Wang, Y. M. (2017). Surface flux transport and the evolution of the sun's polar fields. *Springer Netherlands*, *210*(No. 1–4). https://doi.org/10.1007/s11214-016-0257-0

Webber, W. R., & Lockwood, J. A. (1988). Characteristics of the 22-year modulation of cosmic rays as seen by neutron monitors. *Journal of Geophysical Research*, *93*(A8), 8735. https://doi.org/10.1029/ja093ia08p08735

Weiss, N. O., & Tobias, S. M. (2016). Supermodulation of the Sun's magnetic activity: The effects of symmetry changes. *Monthly Notices of the Royal Astronomical Society*, *456*(3), 2654–2661. https://doi.org/10.1093/mnras/stv2769

Wibberenz, G., & Cane, H. V. (2000). Simple analytical solutions for propagating diffusive barriers and application to the 1974 minicycle. *Journal of Geophysical Research: Space Physics*, *105*(A8), 18315–18325. https://doi.org/10.1029/1999ja000457

Wibberenz, G., le Roux, J. A., Potgieter, M. S., & Bieber, J. W. (1998). Transient effects and disturbed conditions. *Space Science Reviews*, *83*, 309–348. https://doi.org/10.1023/A:1005083109827

Wibberenz, G., Richardson, I. G., & Cane, H. V. (2002). A simple concept for modeling cosmic ray modulation in the inner heliosphere during solar cycles 20-23. *Journal of Geophysical Research*, *107*(A11), 1353. https://doi.org/10.1029/2002JA009461

Wilson, R. M. (1990). On the level of skill in predicting maximum sunspot number: A comparative study of single variate and bivariate precursor techniques. *Solar Physics*, *125*(1), 143–155. https://doi.org/10.1007/BF00154784

Yoshida, A. (2014). Difference between even- and odd-numbered cycles in the predictability of solar activity and prediction of the amplitude of cycle 25. *Annales Geophysicae*, *32*(8), 1035–1042. https://doi.org/10.5194/angeo-32-1035-2014

Zank, G. P., & Frisch, P. C. (1999). Consequences of a Change in the Galactic Environment of the Sun. *The Astrophysical Journal*, *518*, 965–973. https://doi.org/10.1086/307320

Zank, G. P., Matthaeus, W. H., Bieber, J. W., & Moraal, H. (1998). The radial and latitudinal dependence of the cosmic ray diffusion tensor in the heliosphere. *Journal of Geophysical Research: Space Physics*, *103*(A2), 2085–2097. https://doi.org/10.1029/97ja03013